Effect of Pressure on the Selectivity of Supercritical CO_2 Extraction During the Fractionation of a Fatty Acid Ethyl Ester Mixture: Numerical Simulation and Experiment

Sergey V. Mazanov , Almaz U. Aetov * , Alexander S. Zakharov

Posted Date: 4 March 2026

doi: 10.20944/preprints202603.0304.v1

Keywords: supercritical fluid extraction; biodiesel; numerical simulation; fractionation; fatty acid ethyl esters; ethyl oleate; ethyl palmitate

 doi:10.20944/preprints202603.0304.v1

Article

Effect of Pressure on the Selectivity of Supercritical CO_2 Extraction during the Fractionation of a Fatty Acid Ethyl Ester Mixture: Numerical Simulation and Experiment

Sergey V. Mazanov, Almaz U. Aetov * and Alexander S. Zakharov

Institute of Chemical and Petroleum Engineering, Kazan National Research Technological University, Kazan 420015, Russia

* Correspondence: aetovalmaz@mail.ru

Abstract

The high viscosity of biodiesel fuel, caused by the presence of saturated fatty acid esters, limits its application, particularly at low temperatures. Supercritical fluid extraction (SFE) using carbon dioxide represents a promising method for selective fractionation, enabling the removal of high-viscosity saturated components and the enrichment of the fuel with less viscous unsaturated esters. However, the rational design of such processes requires a deep understanding of the interrelationship between flow hydrodynamics, thermodynamic conditions, and mass transfer in a supercritical medium. In this work, a comprehensive computational fluid dynamics (CFD) modeling study of the fractionation process was performed for a model ethyl oleate/ethyl palmitate mixture (25.28:74.72 wt.%) in supercritical CO_2 at pressures of 11 and 14 MPa and a temperature of 40 °C. A three-dimensional model of a laboratory-scale extractor was developed using the ANSYS Fluent software environment. Since the target esters are absent from the standard material database, a custom property library and compiled User-Defined Function (UDF) routines were developed. These describe the temperature dependence of density, viscosity, heat capacity, and thermal conductivity for both the individual components and their mixture using established mixing rules. The calculations employed an Eulerian multiphase model, the realizable k–ε turbulence model, and species transport equations. The modeling revealed pronounced selectivity: under the chosen thermodynamic conditions, ethyl palmitate is extracted preferentially over ethyl oleate, with this difference becoming more pronounced as pressure increases. The developed and verified CFD model deepens the fundamental understanding of hydrodynamics and mass transfer during supercritical fractionation and serves as a basis for optimizing process parameters to produce biodiesel with reduced viscosity. The regime at P=14 MPa and t=40 °C provides the most favorable thermodynamic and hydrodynamic conditions for the selective removal of saturated esters.

Keywords: supercritical fluid extraction; biodiesel; numerical simulation; fractionation; fatty acid ethyl esters; ethyl oleate; ethyl palmitate

1. Introduction

One of the main sources of atmospheric pollution in large cities is motor transport running on fossil fuels. The exhaust gases from such engines contain components hazardous to human health: carbon monoxide (CO), which disrupts tissue respiration; nitrogen oxides (NOx) and sulfur oxides (SOx), causing respiratory diseases; as well as carcinogenic compounds such as polycyclic aromatic hydrocarbons (e.g., benzo(a)pyrene) and soot [1–5]. In light of increasingly stringent environmental regulations and global climate goals, the transition to alternative, cleaner fuels has become highly relevant.

 doi:10.20944/preprints202603.0304.v1

Biodiesel fuel – a mixture primarily composed of methyl or fatty acid ethyl esters (FAEE), obtained mainly through the transesterification of vegetable oils (rapeseed, soybean, palm) or animal fats with lower alcohols (methanol, ethanol) – represents a key renewable energy source [6–10]. Unlike petroleum-based diesel, biodiesel offers several significant environmental advantages: its combustion leads to a substantial reduction in CO emissions, unburnt hydrocarbons, soot, and almost completely eliminates SOx emissions [11–13]. Furthermore, biodiesel is biodegradable and exhibits excellent lubricating properties. The growing demand for environmentally friendly fuel is confirmed by market dynamics: according to a report by the International Energy Agency, published on January 29, 2026, at the India Energy Week exhibition, biofuel production could reach 500-700 million liters per year by 2030 under the main and accelerated scenarios, respectively [14]. Despite these environmental benefits, the widespread commercial adoption of biodiesel is hindered by two groups of problems: technological (high production costs, complexity of removing catalysts and glycerol) and qualitative (instability of properties depending on the feedstock). The latter includes the issue of a high content of high-viscosity saturated fatty acid esters, such as palmitate and stearate, which is characteristic, for example, of biodiesel derived from shea butter or palm oil [1,6,15]. These saturated esters possess a high cloud point and pour point, as well as increased viscosity, unlike esters of unsaturated fatty acids (ethyl oleate, etc.). This directly deteriorates the low-temperature properties of the fuel (cold flow properties), promotes deposit formation in the fuel system, and can lead to non-compliance with stringent quality standards such as EN 14214 (ν=3.5–5.0 mm²/s) or ASTM D6751 (ν=1.9–6.0 mm²/s) [16,17].

The ever-increasing demand for biodiesel necessitates the improvement of technologies to reduce its cost and enhance its quality. A promising direction is the intensification of the transesterification reaction itself, including the use of supercritical fluid media (e.g., supercritical ethanol), which simplifies the process, minimizes catalyst usage, and improves kinetics [18–22]. However, an equally important stage is the subsequent purification and fractionation of the resulting ester mixture to isolate the target high-quality fraction. In this context, supercritical fluid extraction (SFE) based on carbon dioxide ($scCO_2$) stands out as an environmentally friendly, energy-efficient, and highly selective purification technology that does not require organic solvents [23–26]. The process relies on the unique properties of $scCO_2$, which in its supercritical state (Tc = 31.1 °C, Pc = 7.38 MPa) combines liquid-like high density with low viscosity and gas-like high diffusivity [27–29]. These properties can be tuned by varying pressure and temperature, making $scCO_2$ an ideal agent for the selective separation of multicomponent mixtures, such as biodiesel, for the purpose of removing high-viscosity saturated fractions [30–35].

Despite its obvious advantages, the design and optimization of industrial SFE plants for biodiesel fractionation remains a challenging task. This is related to a fundamental problem at the intersection of fluid physics and heat and mass transfer: an insufficient understanding of the interrelationship between the hydrodynamics of the supercritical flow, heat transfer, and the kinetics of selective mass transfer within an extraction column.

As noted in studies devoted to SFE for extracting biologically active compounds, local flow parameters, such as turbulence intensity (TI), have a decisive influence on the wall temperature distribution, density stratification, and, consequently, the efficiency of mass transfer [36–38]. In the context of biodiesel fractionation, this means that flow hydrodynamics (flow structure, mixing) directly determines the separation selectivity of saturated and unsaturated fatty acid esters and, ultimately, the viscosity and low-temperature properties of the final product. In the modern literature, considerable attention is paid to the modeling of SFE processes; however, the emphasis is shifted either towards purely hydrodynamic analysis of apparatus (separators, heat exchangers) [39,40] or the study of processes involving a solid phase (extraction from solid raw materials, aerogel drying) [41–44]. Studies specifically addressing liquid-liquid extraction or fractionation of ester mixtures in $scCO_2$ are often limited to phenomenological models or a simplified approach that does not account for the three-dimensional flow structure and its impact on local selectivity [45–47]. The selection of an adequate multicomponent and multiphase model in computational fluid dynamics

 doi:10.20944/preprints202603.0304.v1

(CFD) is particularly relevant. As shown in comparative studies, approaches such as the Eulerian Multifluid VOF (EMVOF) model can correctly describe complex phase interactions [48–58]. However, their validation and application specifically to the task of selective biodiesel fractionation in $scCO_2$ with product quality prediction remain practically unexplored in the literature.

Consequently, there exists a scientific and technical gap in the field of fundamental CFD modeling that quantitatively links the hydrodynamics of supercritical $scCO_2$ flow with the kinetics of selective mass transfer and the final physicochemical properties of the fractionated fatty acid ester mixture.

The aim of the present work is the development and experimental validation of a comprehensive CFD model for the fractionation process of a mixture of the most common fatty acid esters (FAEE) found in biodiesel, namely ethyl oleate and ethyl palmitate, in supercritical carbon dioxide. The model is aimed at reducing product viscosity through the selective removal of high-viscosity saturated esters. The investigation seeks to deepen the fundamental understanding of the "hydrodynamics-mass transfer-product properties" relationship in supercritical systems and will provide a practical tool for designing energy-efficient and selective technologies for renewable fuel purification

2. Materials and Methods

For the experimental implementation of the fractionation of an ethyl oleate and ethyl palmitate mixture using the $scCO_2$ extraction process, the following reagents were used:

– Carbon dioxide with a purity of not less than 99.0%, LLC "Snabtekhmet" (Kazan, Republic of Tatarstan, Russia);

– Ethyl oleate, pure, Sisco Research Laboratories Pvt. Ltd (Mumbai, Maharashtra, India) (n_D^{20}=1.450, ρ^{20}=870 кг/м^3);

– Ethyl palmitate with a main substance content of not less than 97.0%, LLC TD "KHIMMED" (Moscow, Russia).

The SFE process was implemented on an experimental setup, the schematic diagram and visual appearance of which are presented in Figure 1. The methodology and description of the experiment are detailed in the authors' previous work [59].

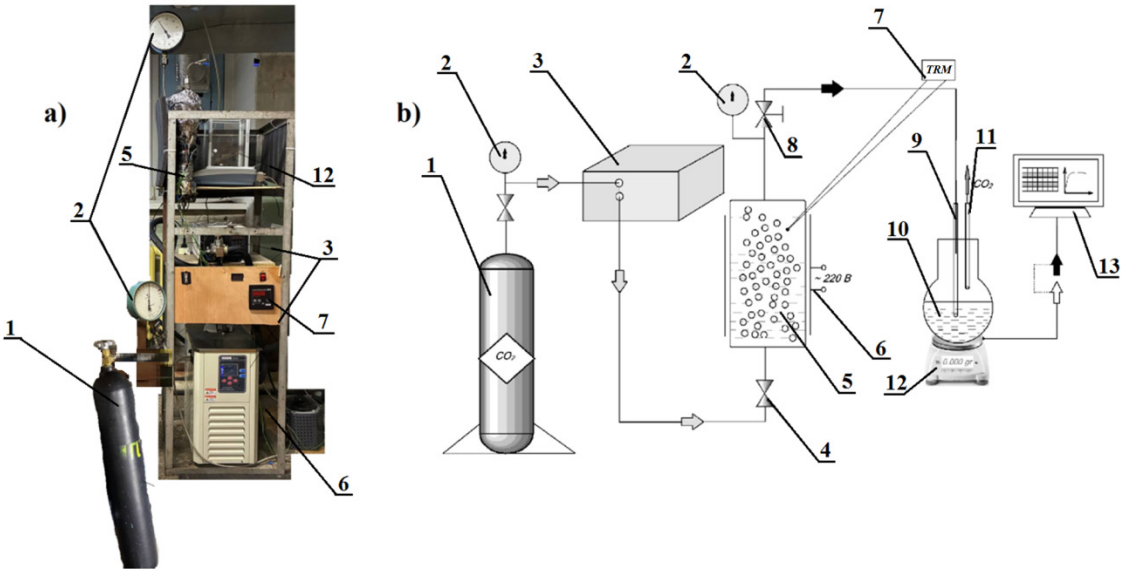

Figure 1. Laboratory-scale supercritical fluid extraction setup designed for the fractionation of fatty acid ethyl esters: a) external view; b) experimental schematic: 1 – gas cylinder; 2 – pressure gauge; 3 – high-pressure pump; 4 – extractor inlet valve; 5 – extractor; 6 – heater; 7 – temperature sensor (thermocouple); 8 – extractor outlet

 doi:10.20944/preprints202603.0304.v1

regulating valve; 9 – delivery tube to glass flask; 10 – glass flask; 11 – gas outlet tube; 12 – electronic laboratory balance with automatic recording; 13 – personal computer.

Analysis of the obtained extract samples for the FAEE mixtures was performed using a "Chromatek-Crystal 5000" gas chromatograph (CJSC SKB "Khromatek", Yoshkar-Ola, Republic of Mari El, Russia). Samples were preliminarily dissolved in isopropanol at a 1:1 mass ratio. Heating was carried out from 40 to 210 °C, increasing the temperature at a rate of 10 °C/min. The injected sample volume was 0.5 μL.

When conducting CFD modeling in Ansys Fluent, the object of the study was the laboratory SFE setup. Figure 2 shows the extractor drawing (a), based on which the geometry was constructed with the indication of the experimental boundary conditions (b).

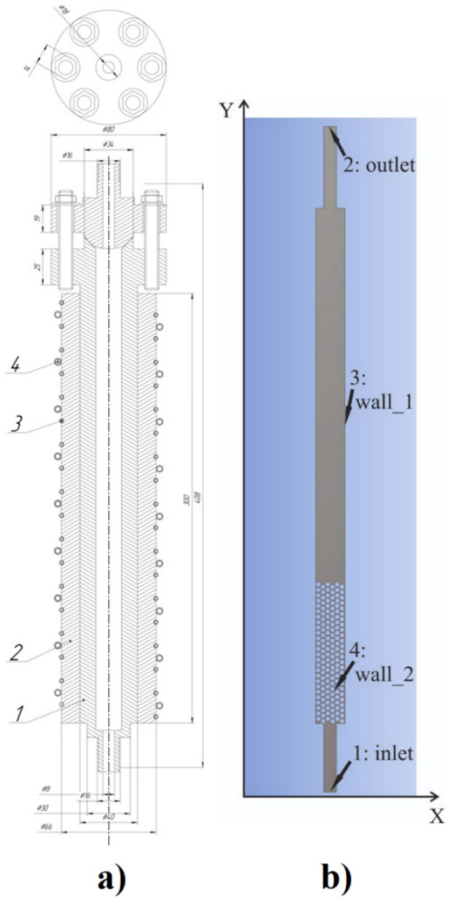

Figure 2. Schematic diagram of the supercritical CO_2 extractor (a): 1 – extractor wall; 2 – insulation; 3 – heater; 4 – CO_2 supply preheating coil; and the extractor geometry (b) indicating the boundary conditions, where: 1: inlet – $scCO_2$ supply; 2: outlet – extract outlet; 3: wall_1 – reactor wall made of AISI 321 steel; 4: wall_2 – packing made of borosilicate glass.

The computational mesh for the extractor model was developed considering the geometric features of the extractor and the requirements for modeling multiphase flows under supercritical conditions, based on the conducted literature review [39–44,48–58]. It consists of 418,639 nodes and 135,929 cells. The input and dimensional data, as well as the boundary conditions and assumptions, are provided in Table 1.

Table 1. Input data and assumptions.

Extractor Dimensions (Figure 2a)		**CFD Modeling Boundary Conditions (Figure 2b)**		
Parameter	**Value**	**Boundary**	**Condition Type**	**Parameters**
Length, mm	408	1: intel	Mass flow Inlet	2 mL/min

 doi:10.20944/preprints202603.0304.v1

Internal diameter, mm	16	2: outlet	Pressure Outlet	11 и 14 MPa
Total internal volume, L	0.092	3: wall_1 4: wall_2	No-Slip wall No-Slip wall	Adiabatic Adiabatic
System				
Extractant	$scCO_2$			
Target component	Mixture of ethyl oleate and ethyl palmitate (25/75 vol.%, 25.28/74.72 wt.%)	Assumptions	Isothermal process (temperature constant throughout the volume)	
Thermodynamic parameters				
Critical point of CO_2	t_c = 31.1 °C, P_c = 7.38 MPa		Viscosity of $scCO_2$ depends on T and P	
Operating range				
Temperature, °C	40		Absence of chemical reactions (purely physical extraction)	
Pressure, МПа	11 and 14			

AISI 321 stainless steel was specified as the extractor material, and borosilicate glass was specified as the material for the packing. The $scCO_2$ supply flow rate was 2 mL/min. The mixture of ethyl oleate and ethyl palmitate (25.28/74.72 wt.%) was used as the target component. The choice of a 2 mL/min flow rate and this volume ratio was based on previous experimental extraction studies. The selection of pressures of 11 and 14 MPa is based on the phase diagrams of the binary mixtures CO_2-ethyl palmitate and CO_2-ethyl oleate (Figure 3), where at these pressures, type I-II phase behavior according to the Williams classification [60] is formed, with unbroken critical curves and the presence of critical points at these pressures and t = 40 °C.

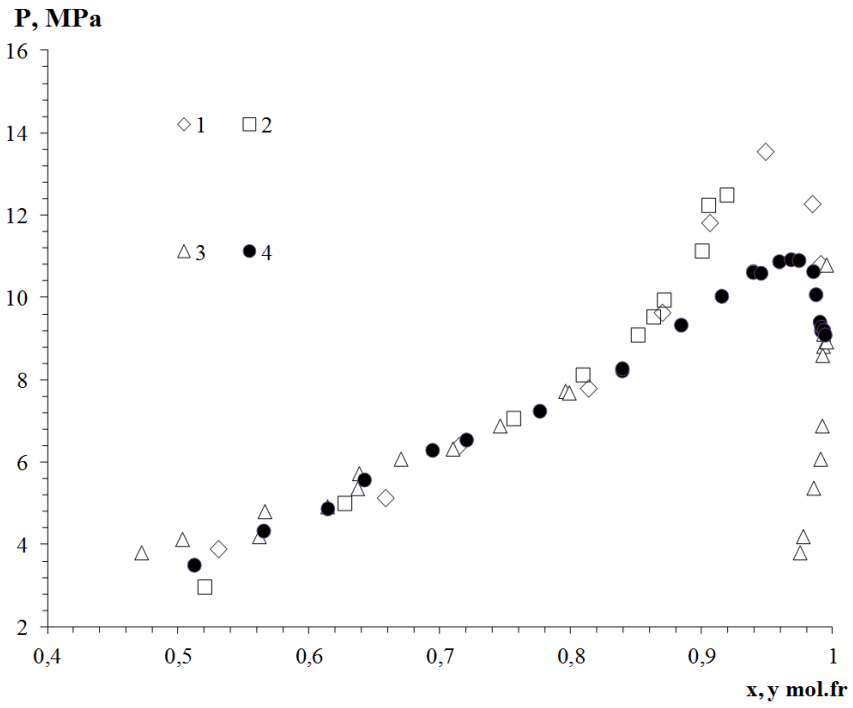

Figure 3. Phase equilibrium diagrams (t = 40 °C) for binary systems: "CO_2-ethyl oleate": 1 – [61], 2 – [62], 3 – [62]; "CO_2-ethyl palmitate": 4 – [63].

 doi:10.20944/preprints202603.0304.v1

The following main equations and models were used in the CFD modeling:
– Continuity equation (mass balance) for each phase:

$$S_i = \frac{\partial(\alpha_i \rho_i)}{\partial t} + \nabla \cdot (\alpha_i \rho_i u_i) \quad (1)$$

where: α_i – volume fraction of phase i, ϱ_i – density of phase i; u_i – velocity of phase i; S_i – mass transfer source term.

– Navier-Stokes equation (momentum balance) for the multiphase system.

$$\frac{\partial(\alpha_i \rho_i u_i)}{\partial t} + \nabla \cdot (\alpha_i \rho_i u_i) = -\alpha_i \nabla P + \nabla \tau_i + \alpha_i \rho_i g + F_{drag} \quad (2)$$

where: P – pressure; $\boldsymbol{\tau}_i$ – viscous stress tensor; F_{drag} – interphase drag force;
– Species transport equation (concentration of the FAEE mixture in $scCO_2$).

$$\frac{\partial(\alpha_{co_2} \rho_{co_2} Y_{FAEE})}{\partial t} + \nabla \cdot (\alpha_{co_2} \rho_{co_2} u_{co_2} Y_{FAEE}) = \nabla \cdot (D_{Eff.} \nabla Y_{FAEE}) + R_{Ext.} \quad (3)$$

where: Y_{FAEE} – mass fraction of the FAEE mixture, D_{Eff} – effective diffusion coefficient, R_{Ext} – extraction rate.

Furthermore, interphase interaction models were considered, such as the drag force between $scCO_2$ and the FAEE mixture:

– Schiller-Naumann model:

$$F = \frac{3}{4} C_D \frac{\alpha_{co_2} \alpha_{FAEE} \rho_{co_2}}{d_p} \cdot |u_{co_2} - u_{FAEE}| \cdot (u_{co_2} - u_{FAEE}) \quad (4)$$

where: C_D – drag coefficient, dependent on the Reynolds number.
– Mass transfer model – LDF (Linear Driving Force):

$$R_{Ext.} = k_m (Y_{FAEE,eq} - Y_{FAEE}) \quad (5)$$

where: k_m – mass transfer coefficient, which for the conditions of this work can be assumed to be in the range from $4 \cdot 10^{-3}$ to $7 \cdot 10^{-2}$ s^{-1}; $Y_{FAEE,eq}$ – equilibrium concentration of the FAEE mixture in $scCO_2$.

To describe the properties of $scCO_2$ and the FAEE mixture, the Peng-Robinson equation of state was used::

$$P = \frac{RT}{V_m - b} - \frac{a(T)}{V_m^2 + 2bV_m - b^2} \quad (6)$$

where: a, b – parameters depending on the critical properties of the components, V – molar volume.

Subsequently, the solution methods in Ansys Fluent were selected. The choice of solvers was the Pressure-Based Solver (preferred for incompressible/weakly compressible flows) and Phase Coupled SIMPLE (for multiphase problems). Discretization schemes: spatial (second-order upwind for momentum; QUICK for the species transport equation) and temporal (First Order Implicit for stability with larger time steps). The flow regime in this system is laminar; however, in this problem setup, a strictly laminar model led to deteriorated solution stability. Therefore, to account for sub-grid mixing and improve stability, as well as to achieve solution convergence, the "k-ε Realizable" model with "Scalable Wall Functions" was applied to account for near-wall effects.

Within the framework of numerical modeling in ANSYS Fluent, it was necessary to replace the standard library material, used by default to represent the organic phase (diesel vapor), with user-defined materials corresponding to the actual composition of the extracted mixture – ethyl oleate and ethyl palmitate. These compounds are absent from the standard Fluent database, so a user-defined material library and a set of UDF functions were implemented to ensure reproducible property definition without manual data entry in the interface and without being tied to a specific project.

For integration into the calculation environment, a user-defined material database file in the Scheme language (faee_materials.scm) was created, including definitions for the individual

 doi:10.20944/preprints202603.0304.v1

components – ethyl oleate and ethyl palmitate – as well as a separate mixture material faee_25_75, corresponding to the mass ratio of 25.28/74.72 wt.%. This approach allows loading the created materials using Fluent's standard tools and using them in the calculation setup on par with standard materials. During the import stage, reference property values at a fixed temperature are set in the library, ensuring correct initialization of the calculation and ease of unit control.

To account for the temperature dependence of properties in the operating temperature range of –20…100 °C, a compiled UDF module in C was developed. This module is connected to Fluent as a compiled UDF and assigned to the relevant materials via the Materials menu for the following quantities: density, viscosity, heat capacity, and thermal conductivity. The UDF uses analytical approximations based on tabulated data of temperature property profiles, ensuring stable calculation of properties in each computational cell during the iterative solution of the momentum and energy equations. Additionally, a temperature range limit was introduced in the code to prevent incorrect extrapolation beyond the specified interval.

The properties of the faee_25_75 mixture are formed directly in the UDF based on the properties of the individual components using the following mixing rules: heat capacity and thermal conductivity were calculated as mass-weighted averages; density was calculated via specific volume; viscosity was determined using the logarithmic mixing rule.

This approach allows modeling the mixture as a single working fluid without including multicomponent transport, simplifying the problem setup and reducing computational costs while maintaining correct temperature-dependent properties.

After importing the created materials into the calculation project, ethyl oleate and ethyl palmitate (and their mixture faee_25_75) were used as components of the organic phase instead of the surrogate component "diesel vapor". This allowed the calculation to be linked to the actual composition of the extracted product and eliminated the uncertainty associated with the conditional properties of a generalized material. To describe the extraction process, the model included interfacial mass transfer between CO_2 and the organic phase (CO_2 dissolution/absorption), with the composition of the organic phase specified via the created mixture. Thanks to the implemented approach, the calculation setup ensures the correct participation of ethyl oleate and ethyl palmitate (and their binary mixture) in the mass and energy transfer processes during supercritical CO_2 extraction.

It should also be noted that the developed property model has limitations: it is intended for single-phase liquid flow. For the ethyl oleate/ethyl palmitate system at reduced temperatures, crystallization and the appearance of a solid phase are possible; therefore, calculations in the lower part of the range (below the solidification onset temperature) require careful interpretation. If it is necessary to simulate the phase transition in Fluent, it is recommended to use the standard "Solidification & Melting" (enthalpy-porosity) model with specified solidus and liquidus temperatures, or to restrict the calculation to the temperature range corresponding to a stable liquid phase.

The solution was initialized from the inlet, and a fixed number of iterations (1500) was set to guarantee full convergence. Convergence was monitored by the scaled residuals for the continuity, x-, y-, z-velocity, energy, k, and ε equations. Analysis of the convergence history showed that a stable (steady-state) solution was achieved at the 723rd iteration. By this point, the residuals of all equations had fallen below the specified criteria. Simultaneously, the integral parameters (mass flow rate and average temperature) reached a plateau, and their relative change over the subsequent 50 iterations did not exceed 0.1%, indicating complete stabilization of the solution. Further iterations, up to the 1500th, did not lead to any significant changes, confirming the achievement of a convergent solution.

3. Results and Discussion

The conditions and results of the experimental $scCO_2$ extraction separation of the binary mixture composed of ethyl oleate and ethyl palmitate are presented in Figure 4 and Table 2 as averaged values after triplicate experiments.

 doi:10.20944/preprints202603.0304.v1

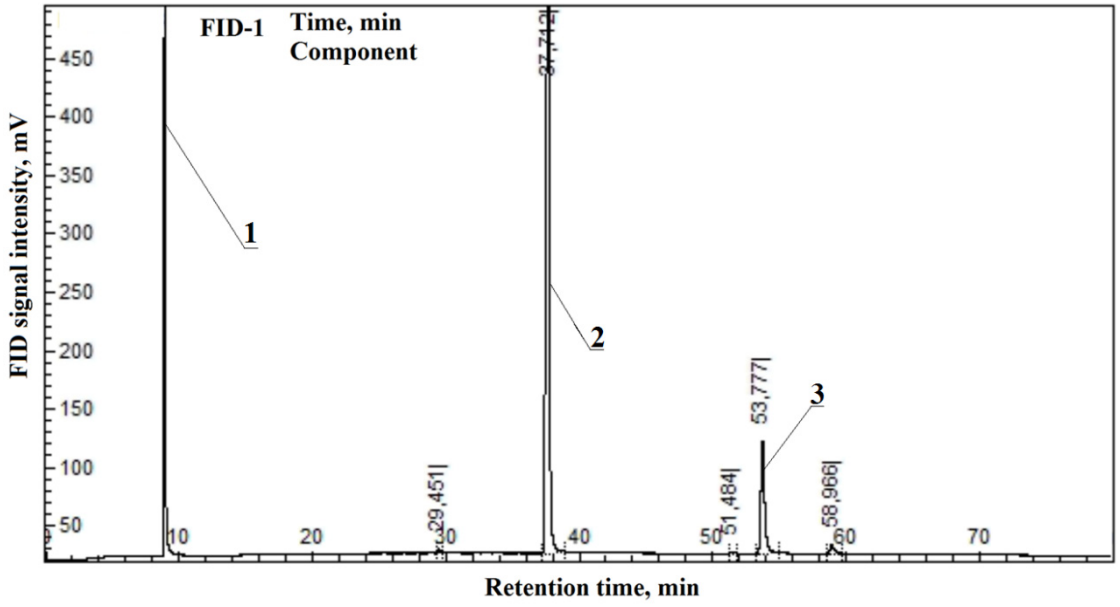

Figure 4. Chromatogram of sample No. 1 (Table 2): 1 – peak corresponding to isopropanol (solvent); 2 – peak corresponding to ethyl palmitate; 3 – peak corresponding to ethyl oleate.

Table 2. Conditions and results of scCO2 extraction separation of the binary mixture composed of ethyl oleate and ethyl palmitate.

N	t, °C	P, MPa	Mixture composition (EO/EP), wt.%	V_{CO_2}, mL/min	τ, min	C_{EP}, wt.%	C_{EO}, wt.%
1	40	11	25.28:74.72	2	15	85.51	14.49
2					30	88.28	11.72
3		14			15	89.66	10.34
4					30	94.34	5.66

* V_{CO_2} – extractant flow rate; C_{EP}, C_{EO} – concentrations of ethyl palmitate and ethyl oleate in the extract, respectively.

The authors established that the selectivity of the extraction separation of the ethyl oleate/ethyl palmitate mixture in supercritical CO_2 can be effectively regulated by varying the pressure and process time. The results presented in Table 2 show that increasing the pressure and the duration of the process leads to an increase in the content of ethyl palmitate in the extract relative to ethyl oleate. This is explained by the fact that, according to the phase diagrams (Figure 3), moving away from the critical point increases the density of the CO_2-ethyl palmitate binary mixture, which is directly related to the increased solubility of this component and, consequently, its yield. Thus, the obtained data have practical significance for the development of technologies aimed at reducing the viscosity of biodiesel fuel.

Statistical processing of the results presented in Table 2 was performed using Student's t-test. The significance of differences between the concentration values of ethyl oleate and ethyl palmitate under different extraction conditions was assessed at a significance level of $p < 0.05$. It was found that increasing the pressure from 11 to 14 MPa at a fixed process time leads to a statistically significant increase in the content of ethyl palmitate in the extract. This confirms the reproducibility of the experiment and the reliability of the identified patterns.

Based on the conducted experiments, the results of numerical modeling of hydrodynamics and heat transfer in the SFE extractor were analyzed for two operating pressures: 11 and 14 MPa, and t =

 doi:10.20944/preprints202603.0304.v1

40 °C. The analysis focused on the fields of key parameters determining the fractionation process of the FAEE mixture: pressure, $scCO_2$ flow velocity, temperature, and the distribution of species mass fractions.

The distribution of static pressure in the apparatus is a key factor determining the density and, consequently, the solvent power of $scCO_2$. Figure 5 shows the pressure fields for the two operating modes.

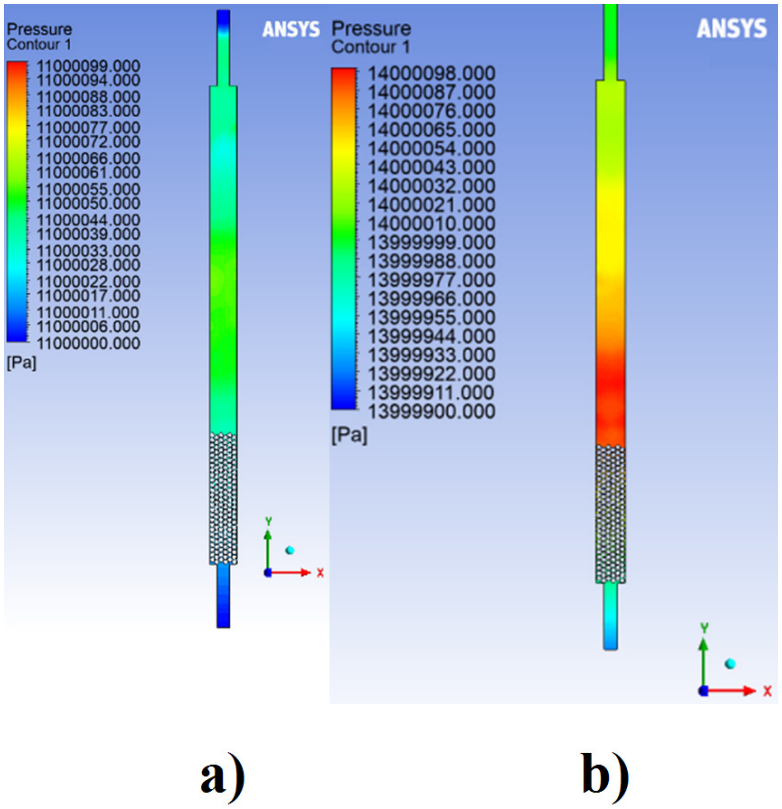

Figure 5. Static pressure distribution (Pa) in the extractor at pressures: a) 11 MPa; b) 14 MPa.

The main pressure drop (hydraulic resistance) occurs in the packing zone, where the flow interacts with the surface of the spheres (Figure 5). At an inlet pressure of 14 MPa, the absolute pressure values throughout the volume are naturally higher than at 11 MPa. However, more importantly, the pressure gradient in the packing zone at 14 MPa is 15-20% higher. This indicates a change in the flow regime and a more uniform penetration of $scCO_2$ through the packing layer at higher pressure, which is favorable for phase contact.

The flow structure directly influences the contact time and the efficiency of mass transfer between $scCO_2$ and the liquid FAEE mixture. Figure 6 presents the $scCO_2$ flow velocity fields.

 doi:10.20944/preprints202603.0304.v1

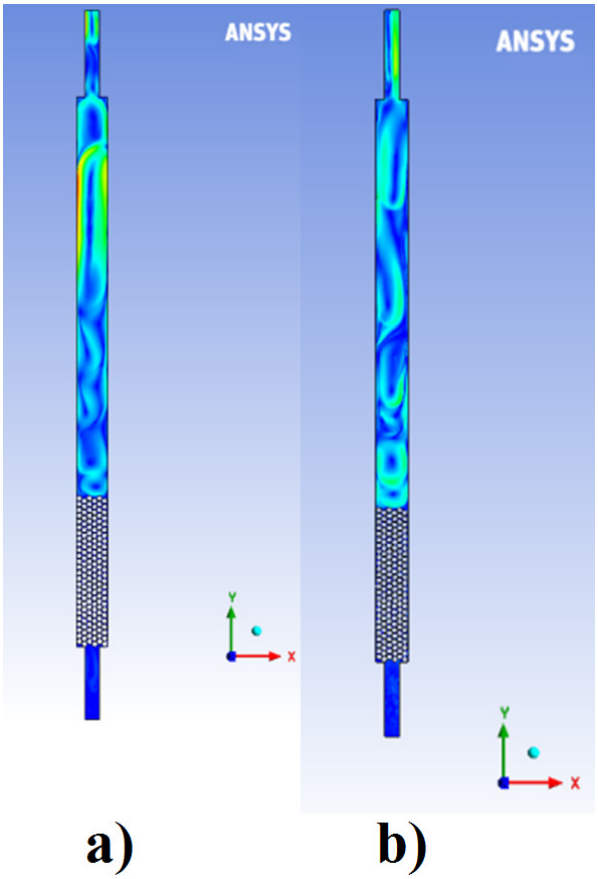

Figure 6. scCO2 flow velocity field in the extractor cross-section at pressures: a) 11 MPa; b) 14 MPa.

Analysis of the velocity fields reveals a significant influence of pressure on hydrodynamics. At 11 MPa, the formation of a pronounced high-velocity channel is observed in the upper-central part of the apparatus, accompanied by the emergence of extensive zones with low velocities near the walls and in the inter-sphere space of the packing. This pattern indicates non-uniform flow distribution and the risk of stagnant zones where mass transfer would be limited.

When the pressure is increased to 14 MPa, the velocity profile becomes significantly more uniform. The average velocity in the inter-sphere channels increases, and the scatter of values across the apparatus cross-section decreases. This is associated with the increase in $scCO_2$ density and, consequently, a decrease in its kinematic viscosity, which promotes more efficient flow distribution. For the fractionation process, a uniform velocity field is critically important as it ensures homogeneous contact of the solvent with the entire mass of the fractionated liquid, prevents premature "breakthrough" of unreacted zones, and facilitates achieving uniform distribution.

To verify the assumption of isothermality of the process and assess the influence of operating parameters on the temperature field inside the extractor, temperature profiles along the apparatus height were analyzed. Figure 7 shows the temperature distributions along the central axis and near the extractor walls for the two investigated pressures – 11 and 14 MPa. Since the modeling results for pressures of 11 and 14 MPa showed coinciding temperature profiles, Figure 7 presents generalized dependencies for both pressures. Line 1 corresponds to the temperature on the central axis, line 2 – near the inner surfaces of the extractor walls.

 doi:10.20944/preprints202603.0304.v1

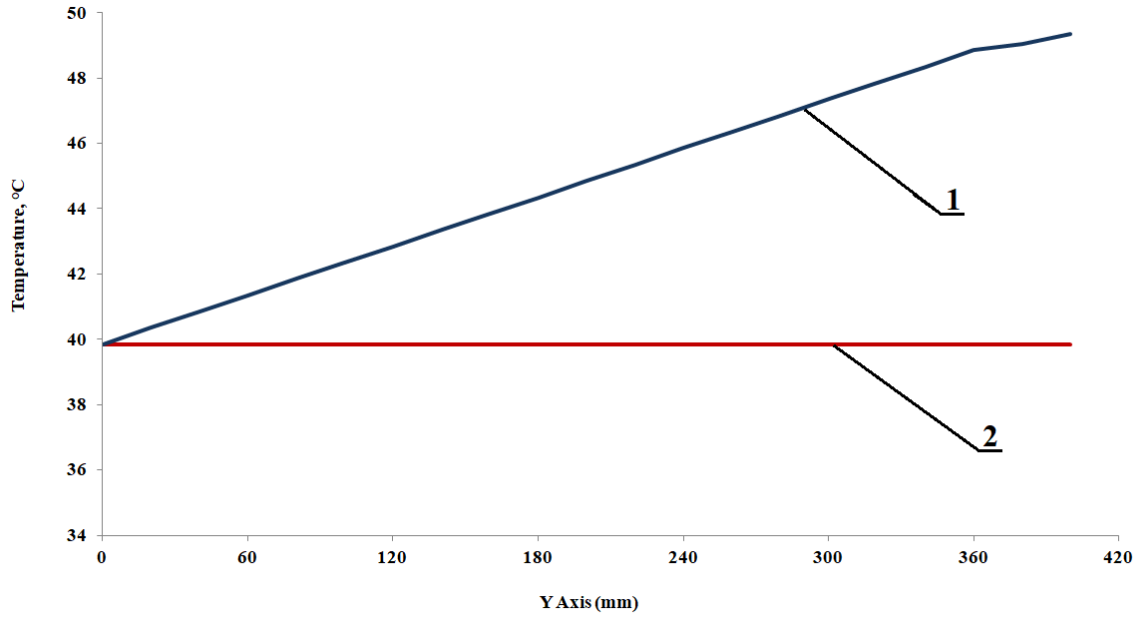

Figure 7. Temperature profiles along the extractor height: 1 – on the central axis (at pressures of 11 and 14 MPa); 2 – near the inner wall surfaces (at pressures of 11 and 14 MPa).

As can be seen from the graph, the temperature at the wall remains practically constant along the entire height and equals the set value, which fully corresponds to the thermostatic boundary condition. Temperature deviations on the central axis may arise due to the compressibility of the working fluid or due to internal (viscous) friction, but with thermostated walls, they are quickly suppressed by heat exchange with the wall. The temperature profiles obtained for pressures of 11 and 14 MPa coincide – the differences between them do not exceed 0.1 °C, which is within the error of the numerical solution. This indicates that, within the framework of the adopted model, the temperature field is determined solely by the boundary conditions and does not depend on the operating pressure in the investigated range. The absence of significant temperature gradients confirms the correctness of the isothermal process assumption and allows, in the further analysis of hydrodynamics and mass transfer, to consider pressure changes as the main factor influencing density, viscosity, and, consequently, the efficiency of fractionation.

The analysis of temperature fields confirmed that the process proceeds under isothermal conditions, and the influence of temperature gradients on the properties of the supercritical fluid is negligible. This allows proceeding to consider the factor directly determining the extraction efficiency – density. It is density, dependent on pressure, that directly affects the solvent power of the fluid and the selectivity of extracting mixture components. Figure 8 shows the density distribution fields in the extractor for the 11 and 14 MPa modes, allowing a visual assessment of the thermodynamic conditions at each point of the apparatus.

 doi:10.20944/preprints202603.0304.v1

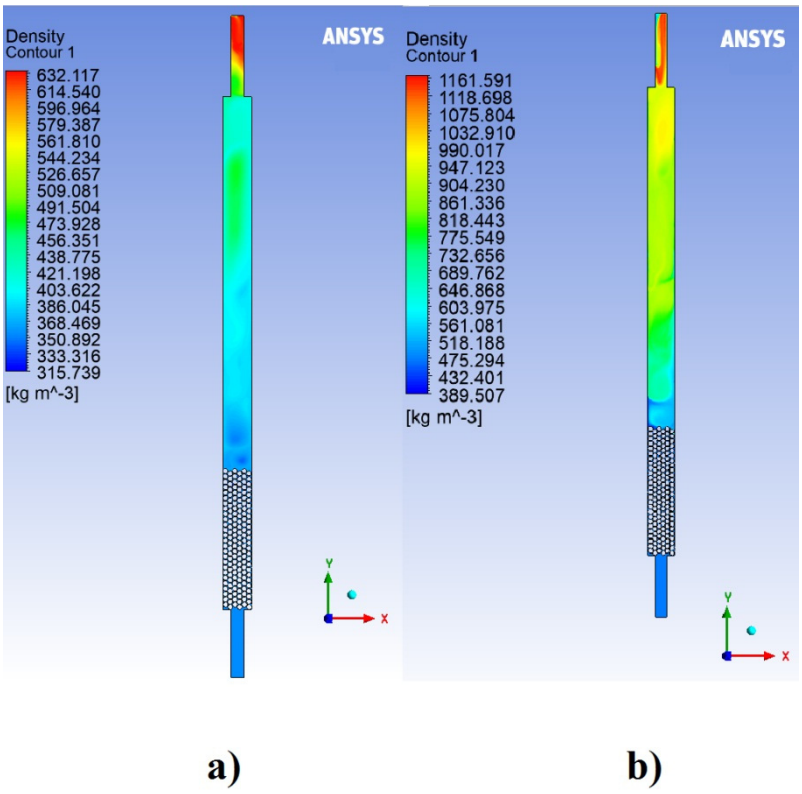

Figure 8. scCO2 density distribution fields in the extractor at pressures of 11 MPa (a) and 14 MPa (b).

Analysis of the density fields allows the following key observations. Throughout the working volume, the density at 14 MPa systematically exceeds the values at 11 MPa, which fully corresponds to thermodynamic expectations. Along the flow direction (from bottom to top), a smooth increase in density is observed, caused by the gradual saturation of CO_2 with esters and the minor influence of hydraulic resistance. The density gradient is more pronounced at 14 MPa, which is associated with the greater compressibility of the medium in this parameter range. In the near-wall zones, the density is somewhat lower than on the central axis, which is explained by the lower intensity of mass transfer near the walls. The difference between the density values at the center and the wall does not exceed 15–20 kg/m³ for both pressures, indicating a relatively uniform density field across the apparatus cross-section and being a favorable factor for the uniform course of the extraction process. The obtained density fields unequivocally show that increasing the operating pressure from 11 to 14 MPa leads to a significant increase in density at all points of the apparatus. Since the solvent power of $scCO_2$ with respect to lipophilic compounds, such as FAEE, has a direct correlation with density, it can be stated that the 14 MPa mode provides a higher extraction potential. This conclusion, based on the visualization of density fields, creates a solid thermodynamic basis for interpreting the possible increase in yield and selectivity in this mode.

After establishing the patterns of distribution of parameters determining the thermodynamic state of the system, the next stage was the analysis of mass transfer – the process responsible for the selective extraction of target components. For this purpose, separate CFD calculations of the transport of ethyl oleate and ethyl palmitate in supercritical CO_2 at pressures of 11 and 14 MPa were performed. Figure 9 shows the obtained profiles of the mass fraction distribution of ethyl oleate and ethyl palmitate along the extractor height. For each pressure, dependencies are presented reflecting the change in concentration of these components along the central axis and averaged values for the near-wall region (left and right walls). Since the mass fraction of carbon dioxide at each point is determined as the complement to unity, it is not shown in the figure. The presented dependencies provide a quantitative representation of the process selectivity and allow linking the observed changes in composition with the hydrodynamic and thermodynamic conditions discussed earlier. Averaging

 doi:10.20944/preprints202603.0304.v1

the values for both walls allows assessing the transverse non-uniformity of component distribution across the apparatus cross-section. The mass fraction values in Figure 9 are given relative to the zero level at the extractor inlet, which allows a clear visualization of the accumulation dynamics of each component along the apparatus height.

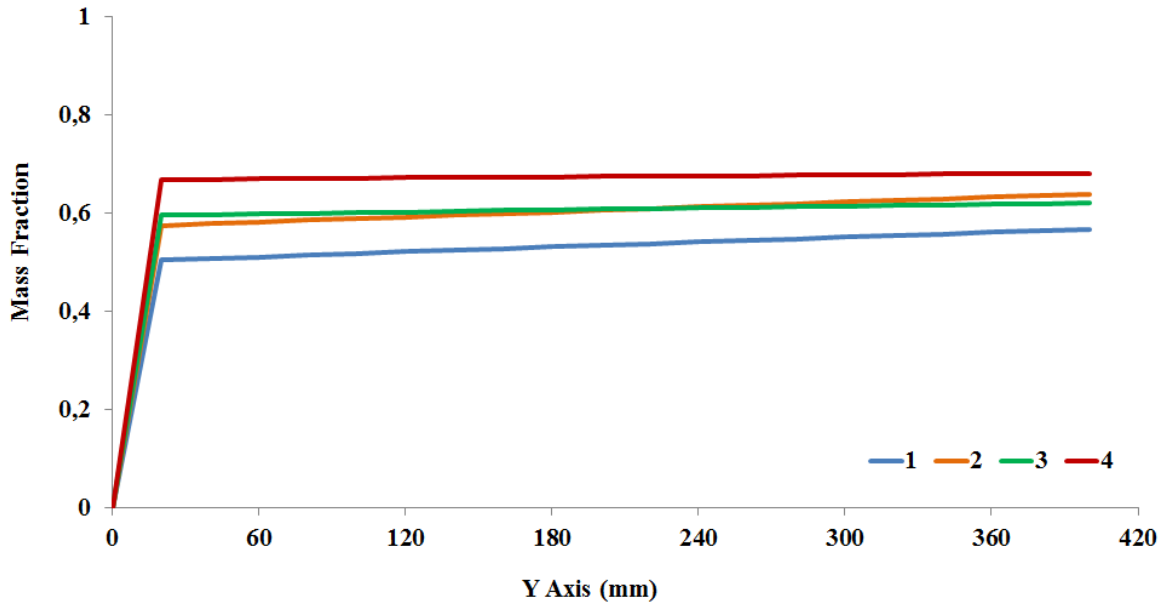

Figure 9. Profiles of component mass fraction distribution along the extractor height at pressures of 11 and 14 MPa: 1 – ethyl oleate (11 MPa); 2 – ethyl palmitate (11 MPa); 3 – ethyl oleate (14 MPa); 4 – ethyl palmitate (14 MPa).

Analysis of the component mass fraction distribution profiles (Figure 9) allows drawing the following conclusions: at a pressure of 11 MPa, the mass fraction of ethyl palmitate at the extractor outlet (Y = 380–400 mm) reaches 0.69, while the fraction of ethyl oleate is 0.51. This indicates the preferential extraction of the saturated ester – ethyl palmitate – under these conditions. Increasing the pressure to 14 MPa leads to an even more pronounced increase in palmitate concentration: its mass fraction rises to 0.76, whereas the fraction of oleate increases only to 0.58. Thus, throughout the entire apparatus height, the content of ethyl palmitate in the extract consistently exceeds that of ethyl oleate, and this difference amplifies with increasing pressure.

The identified pattern is explained by the difference in the solubility of the components in supercritical CO_2. According to the phase diagrams (Figure 3), ethyl palmitate exhibits higher solubility in the investigated parameter range, which determines its preferential extraction. Increasing the pressure further increases the density of CO_2 and, consequently, its solvent power, which particularly affects the more soluble component – ethyl palmitate. Thus, both the calculated and experimental data confirm that the $scCO_2$ extraction process allows for the efficient separation of the binary ester mixture, enriching the extract with the high-viscosity saturated component – ethyl palmitate – and the raffinate with the fraction enriched in unsaturated ethyl oleate having reduced viscosity. This directly corresponds to the aim of the work – reducing the viscosity of biodiesel fuel.

4. Conclusion

This study addressed the pressing issue of improving biodiesel quality by reducing its viscosity through the selective removal of high-viscosity saturated fatty acid esters from a mixture with unsaturated esters. Fractionation using supercritical carbon dioxide was proposed as a promising method, the efficiency of which directly depends on the hydrodynamic and thermodynamic conditions within the extractor. A three-dimensional CFD model of the supercritical extraction

 doi:10.20944/preprints202603.0304.v1

process was developed and experimentally verified for a laboratory-scale extractor with a volume of 0.092 L using the ANSYS Fluent software environment. Since the target components – ethyl oleate and ethyl palmitate – are absent from the standard material database, a custom property library and compiled User-Defined Function (UDF) routines were implemented for the first time. These enable the reproducible specification of temperature-dependent density, viscosity, heat capacity, and thermal conductivity for both the individual substances and their binary mixture using mixing rules, ensuring a physically correct description of the working fluid's properties.

A comparative CFD modeling study was conducted for two operating pressures – 11 and 14 MPa – at a constant temperature of 40 °C. Analysis of the pressure, velocity, temperature, and density fields, as well as the distributions of component mass fractions, revealed a comprehensive positive effect of increasing pressure on the process. Increasing the pressure to 14 MPa led to a 15–20% increase in density throughout the extractor volume. Considering the direct correlation between density and solvent power, this creates a fundamentally higher extraction potential. Concurrently, a homogenization of the flow velocity field was observed, along with a reduction in hydraulic resistance within the packing layer and a decrease in the extent of stagnant zones. These changes promote more uniform and intensive contact between phases, which is critically important for efficient mass transfer.

Both the calculated and experimental data confirm that ethyl palmitate is extracted preferentially over ethyl oleate, and this selectivity intensifies with increasing pressure. The mass fraction of ethyl palmitate at the extractor outlet increases from 0.69 at 11 MPa to 0.76 at 14 MPa, while the fraction of ethyl oleate only rises from 0.51 to 0.58. Experimental concentrations at 14 MPa and an extraction time of 30 min reach 94.3 wt.% for ethyl palmitate and 5.7 wt.% for ethyl oleate, showing good agreement with the calculated profiles. The mass fraction of the target ester mixture in the extract increases by 9.5 wt.% upon raising the pressure, providing quantitative confirmation of process intensification.

Author Contributions: Conceptualization, S.V.M. and A.U.A.; methodology, S.V.M. and A.S.Z.; software, A.S.Z.; validation, S.V.M., A.U.A. and A.S.Z.; formal analysis, A.U.A.; investigation, S.V.M. and A.S.Z.; resources, S.V.M.; data curation, A.S.Z.; writing—original draft preparation, S.V.M. and A.S.Z.; writing—review and editing, A.U.A.; visualization, A.S.Z.; supervision, S.V.M.; project administration, A.U.A.; funding acquisition, S.V.M. All authors have read and agreed to the published version of the manuscript.

Acknowledgments: The work was carried out with financial support from the Russian Science Foundation (project No. 23-79-10304, https://rscf.ru/project/23-79-10304/).

Conflicts of Interest: The authors declare no conflicts of in-terest.

References

1. Shapovalov, Y.A.; Mazanov, S.V.; Aetov, A.U.; Kamysbaev, D.H.; Tokpayev, R.R.; Gumerov, F.M. Separation of Rapeseed Oil Transesterification Reaction Product Obtained Under Supercritical Fluid Conditions Using Heterogeneous Catalysts. Energies **2025**, 18, 1669. https://doi.org/10.3390/en18071669
2. Mazanov, S.V.; Kouagou, Z.-M.; Hounkpatin, D.D.; Fonkou, M.J.; Usmanov, R.A.; Zaripov, Z.I.; Gumerov, F.M.; Shapovalov, Y.A. Transesterification of Shea (Karite) and Palm Oils in Supercritical Ethanol. Russ. J. Phys. Chem. B **2022**, 16, 1347–1353. https://doi.org/ 10.1134/S1990793122080127
3. Usmanov, R.A.; Mazanov, S.V.; Gabitova, A.R.; Miftakhova, L.K.; Gumerov, F.M.; Musin, R.Z.; Abdulagatov, I.M. The effect of fatty acid ethyl esters concentration on the kinematic viscosity of biodiesel fuel. J. Chem. Eng. Data **2015**, 60, 3404–3413. https://doi.org/10.1021/acs.jced.5b00683
4. Gabitova, A.R.; Mazanov, S.V.; Usmanov, R.A.; Zaripov, Z.I.; Gumerov, F.M.; Abdulagatov, I.M. Viscometry as a method for determining concentration of fatty acid ethyl esters in biodiesel fuel. Chem. Technol. Fuels Oils **2017**, 53, 77–86. https://doi.org/10.1007/s10553-017-0783-9

 doi:10.20944/preprints202603.0304.v1

5. Mazanov, S.V.; Gabitova, A.R.; Miftahova, L.K.; Usmanov, R.A.; Gumerov, F.M.; Zaripov, Z.I.; Vasil'ev, V.A.; Karalyn, E.A. Preparing biodiesel fuel in supercritical fluid conditions with heterogeneous catalysts. Russ. J. Phys. Chem. B **2016**, 10, 1099–1107. https://doi.org/10.1134/S1990793116070137
6. Mazanov, S.V.; Usmanov, R.A.; Kuagu, J.M.; Unkpaten, D.D.; Fonkou, M.D.; Gumerov, F.M.; Zaripov, Z.I.; Shapovalov, Y.A.; Nauryzbayev, M.K. Experimental study of non-catalytic and catalytic reaction of transesterification of rapeseed oil under supercritical fluid conditions in a flow-type installation. Ind. Kazakhstan **2019**, 1, 90–92.
7. Rozina; Ahmad, M.; Zafar, M.; Sultana, S.; et al. Biodiesel. In Hydrogen and Low-Carbon Fuels in Circular Bio-economy: Assessment Methodologies, Production Technologies and Sector-Specific Applications; Springer: Cham, Switzerland, **2025**; pp. 209–229.
8. Pedraza-Casanova, L.; Bautista, L.F.; Vicente, G.; et al. An in Silico Environmental Risk Assessment of Palm Oil Transesterification in Supercritical Ethanol as a Tool to Enhance Sustainable Biofuel Production. J. Supercrit. Fluids **2025**, 106724. https://doi.org/10.1016/j.supflu.2025.106724
9. Kamjam, M.; Prommajak, T.; Punsuvon, V.; et al. Valorization of Rambutan Seed Waste into Biodiesel via Non-Catalytic Supercritical Ethanol and Ethyl Acetate. Energies **2025**, 18, 6004. https://doi.org/10.3390/en18226004
10. Perumal, G.; Palanisamy, S.; Sivaprakasam, S.; et al. A systematic review on the production of biodiesel using various feedstocks and effective catalysts. Pet. Sci. Technol. **2025**, 43, 1910–**1926**. https://doi.org/10.1080/10916466.2024.2366464
11. Guduru, V.R.R.; Sharma, A.; Singh, R.; et al. A comprehensive review on biodiesel performance: advantages, challenges, policies and prospects. Int. J. Oil Gas Coal Technol. **2025**, 38, 240–282.
12. Onwusa, S.C.; Nwosu, C.; Okoro, E.; et al. Performance and Emission Analysis of Biodiesel Blends in Diesel Engines: Comprehensive Review. Unizik J. Technol. Prod. Mech. Syst. **2025**, 7, 355–371.
13. Pandey, R.K.; Singh, A.K.; Srivastava, S.P.; et al. Decarbonizing Transportation: Navigating the Nexus of Greenhouse Gas Emissions, Advanced Mixed Biofuels, and Mixed CNG–Hydrogen Gas. In Green Hydrogen Production; CRC Press: Boca Raton, FL, USA, **2025**; pp. 326–344.
14. OilWorld.ru. Biofuel production could reach 500–700 million liters per year by **2030**. Available online: https://www.oilworld.ru/analytics/forecast/365813 (accessed on 29 January 2026).
15. Usmanov, R.A.; Zaripov, Z.I.; Mazanov, S.V.; et al. Transesterification of oils with high contents of saturated and unsaturated fatty acids in supercritical fluid conditions. Braz. J. Chem. Eng. **2025**, 1–12. https://doi.org/ 10.1007/s43153-025-00540-9
16. EN 14214:2013 V2+A2:2019; Liquid Petroleum Products—Fatty Acid Methyl Esters (FAME) for Use in Diesel Engines and Heating Applications—Requirements and Test Methods. European Committee for Standardization: Brussels, Belgium, **2019**.
17. ASTM D6751-23a; Standard Specification for Biodiesel Fuel Blendstock (B100) for Middle Distillate Fuels. ASTM International: West Conshohocken, PA, USA, **2023**. https://doi.org/10.1520/D6751-23A
18. Farouk, S.M.; Ahmed, M.A.; Hassan, H.M.; et al. Recent advances in transesterification for sustainable biodiesel production, challenges, and prospects: a comprehensive review. Environ. Sci. Pollut. Res. **2024**, 31, 12722–12747. https://doi.org/10.1007/s11356-024-32027-4
19. Taher, H.; Al-Zuhair, S.; Al-Marzouqi, A.H.; et al. A Review of Enzymatic Transesterification of Microalgal Oil-Based Biodiesel Using Supercritical Technology. Enzyme Res. **2011**, 468292. https://doi.org/10.4061/2011/468292
20. Badday, A.S.; Abdullah, A.Z.; Lee, K.T. Intensification of biodiesel production via ultrasonic-assisted process: A critical review on fundamentals and recent development. Renew. Sustain. Energy Rev. **2012**, 16, 4574–4587. https://doi.org/10.1016/j.rser.2012.04.057
21. Subramaniam, B. Enhancing the stability of porous catalysts with supercritical reaction media. Appl. Catal. A Gen. **2001**, 212, 199–213.
22. Hoff, K.L.; Eisenacher, M. Process intensification strategies for esterification: kinetic modeling, reactor design, and sustainable applications. Int. J. Mol. Sci. **2025**, 26, 7214. https://doi.org/10.3390/ijms26157214
23. Zaripov, Z.I.; Mazanov, S.V.; Nakipov, R.R.; Solovyova, A.O.; Aetov, A.U.; Monakhov, I.I. Investigation of Phase Equilibria of Binary Systems Target Component (Ethyl Acetate, Ethyl Oleate, Ethyl Palmitate) –

 doi:10.20944/preprints202603.0304.v1

Extractant (Carbon Dioxide, Ethane, Refrigerant R404A). Inzhenernaya Fizika **2025**, 10, 17–26. https://doi.org/10.25791/infizik.10.2025.1507

24. Zaripov, Z.I.; Nakipov, R.R.; Usmanov, R.A.; Aetov, A.U.; Gumerov, F.M. Phase Behavior of the Binary System Refrigerant R404A-Acetone and SFE Extraction of Acetone from Aqueous Solution with Refrigerant R404A. Supercritical Fluids: Theory and Practice **2025**, 20, 22–33. https://doi.org/10.34984/SCFTP.2025.20.3.002
25. Ramsey, E.; Sun, Q.; Zhang, Z.; Zhang, C.; Gou, W. Mini-Review: Green sustainable processes using supercritical fluid carbon dioxide. J. Environ. Sci. **2009**, 21, 720–726. https://doi.org/10.1016/S1001-0742(08)62330-X
26. Liu, H.; Yang, Y.; Xu, L.; et al. Role of supercritical carbon dioxide ($scCO_2$) in fabrication of inorganic-based materials: a green and unique route. Sci. Technol. Adv. Mater. **2021**, 22, 695–717. https://doi.org/10.1080/14686996.2021.1955601
27. Uchida, H.; Izaki, K.; Shiokawa, M. Chemical deposition of silica-based thin films under supercritical carbon dioxide atmosphere using tetraethylorthosilicate precursor with oxidizing agents. J. Ceram. Soc. Jpn. **2016**, 124, 18–22. https://doi.org/10.2109/jcersj2.15202
28. Liu, R.; Zhang, P.; Zhang, S.; et al. Ionic liquids and supercritical carbon dioxide: green and alternative reaction media for chemical processes. Rev. Chem. Eng. **2016**, 32, 587–609. https://doi.org/10.1515/revce-2015-0078
29. Medina-Gonzalez, Y.; Camy, S.; Condoret, J.S. Cellulosic materials as biopolymers and supercritical CO2 as a green process: chemistry and applications. Int. J. Sustain. Eng. **2012**, 5, 47–65. https://doi.org/10.1080/19397038.2011.613488
30. Knez, Ž.; Markočič, E.; Leitgeb, M.; Primožič, M.; Knez Hrnčič, M.; Škerget, M. Industrial applications of supercritical fluids: A review. Energy **2014**, 77, 235–243. https://doi.org/10.1016/j.energy.2014.07.044
31. Hajareh Haghighi, F.; Farhadian, M.; Gholami, M.; et al. Magnetic iron oxide nanomaterials for lipase immobilization: promising industrial catalysts for biodiesel production. Catalysts **2024**, 14, 336.
32. Lin Htun, S.; Adair, J.; Goldfarb, J.L. Chemical and biological solutions to the thermodynamic challenges posed by hydrothermal liquefaction process water. Prog. Energy **2025**, 7, 032003.
33. Saini, R.; Kumar, S.; Sharma, P.; et al. Deep eutectic solvents: The new generation sustainable and safe extraction systems for bioactive compounds in agri food sector: An update. J. Food Process. Preserv. **2022**, 46, e16250. https://doi.org/10.1111/jfpp.16250
34. Neto, B.A.D.; Lapis, A.A.M.; Souza, R.Y. Task-specific ionic liquids: design, properties, and applications. In Encyclopedia of Ionic Liquids; Springer: Singapore, **2023**; pp. 1273–1283. https://doi.org/10.1007/978-981-33-4221-7_33
35. Bermudez, G.; Sánchez, M.; Pérez, A.; et al. Extraction and analytical methods for the characterization of polyphenols in marine microalgae: A review. Mar. Drugs **2024**, 22, 538. https://doi.org/10.3390/md22120538
36. Uwineza, P.A.; Waśkiewicz, A. Recent Advances in Supercritical Fluid Extraction of Natural Bioactive Compounds from Natural Plant Materials. Molecules **2020**, 25, 3847. https://doi.org/10.3390/molecules25173847
37. Bhadange, Y.A.; Carpenter, J.; Saharan, V.K. A comprehensive review on advanced extraction techniques for retrieving bioactive components from natural sources. ACS Omega **2024**, 9, 31274–31297. https://doi.org/10.1021/acsomega.4c02718
38. Vafaei, N.; Naderi, M.; Esmaeilzadeh, F.; et al. Application of supercritical fluid extraction (SFE) of tocopherols and carotenoids (hydrophobic antioxidants) compared to non-SFE methods. AppliedChem **2022**, 2, 68–92. https://doi.org/10.3390/appliedchem2020005
39. Alcântara, S.C.S.; Mendes, R.L.; et al. Critical Review of Advances and Numerical Modeling in Absorbers and Desorbers of Absorption Chillers: CFD Applications, Constraints, and Future Prospects. Energies **2025**, 18, 314. https://doi.org/10.3390/en18020314
40. Spitas, C.; Amani, A.; Spitas, V. A review of emerging computational models for the design of smart structures and powertrains. J. Coupled Syst. Multiscale Dyn. **2015**, 3, 279–332. https://doi.org/10.1166/jcsmd.2015.1090

 doi:10.20944/preprints202603.0304.v1

41. García-González, C.A.; Budtova, T.; Smirnova, I.; et al. Review and perspectives on the sustainability of organic aerogels. ACS Sustain. Chem. Eng. **2025**, 13, 6469–6492.
42. Smirnova, I.; Gurikov, P. Aerogel production: Current status, research directions, and future opportunities. J. Supercrit. Fluids **2018**, 134, 228–233. https://doi.org/10.1016/j.supflu.2017.12.037
43. Turhan Kara, I.; Erkey, C.; et al. Life cycle assessment of aerogels: a critical review. J. Sol-Gel Sci. Technol. **2024**, 111, 618–649. https://doi.org/10.1007/s10971-024-06455-0
44. Spietelun, A.; Pilarczyk, M.; Kloskowski, A.; Namieśnik, J. Understanding solid-phase microextraction: key factors influencing the extraction process and trends in improving the technique. Chem. Rev. **2013**, 113, 1667–1685. https://doi.org/10.1021/cr300148j
45. Shen, J.; Zhang, Y.; Li, W.; et al. Advancements in the singlemer separation of polymethoxyflavones in citrus peels. J. Food Bioact. **2025**, 29. https://doi.org/10.26599/JFB.2025.95029401
46. Boh, B. Ganoderma lucidum: a potential for biotechnological production of anti-cancer and immunomodulatory drugs. In Topics in Anti-Cancer Research: Volume 3; Bentham Science: **2014**; pp. 202–271. https://doi.org/10.2174/1574891x113089990036
47. Pownceby, H.; Rahman, M.; Islam, S.; et al. Extraction of Rare Earth Elements from Monazite: A Review of Current Practices and Emerging Opportunities for Bangladesh. **2025**. (Preprint / Technical report).
48. Wang, F.Z.; Zhang, L.; Chen, X.; et al. Recent advancements in fluid dynamics: drag reduction, lift generation, computational fluid dynamics, turbulence modelling, and multiphase flow. Arab. J. Sci. Eng. **2024**, 49, 10237–10249. https://doi.org/10.1007/s13369-024-08945-3
49. Soodmand, A.M.; Hosseini, S.M.; Ahmadi, G. A comprehensive review of computational fluid dynamics simulation studies in phase change materials: applications, materials, and geometries. J. Therm. Anal. Calorim. **2023**, 148, 10595–10644. https://doi.org/10.1007/s10973-023-12438-0
50. Santra, S.; Mandal, S.; Chakraborty, S. Phase-field modeling of multicomponent and multiphase flows in microfluidic systems: A review. Int. J. Numer. Methods Heat Fluid Flow **2021**, 31, 3089–3131. https://doi.org/10.1108/HFF-01-2020-0001
51. Lam, W.Y.; Khoo, B.C.; Lim, T.T. Reviewing two-phase flow modeling in membrane processes through computational fluid dynamics. Chem. Eng. Res. Des. **2025**, 214, 28–38.
52. Nadamani, M.N.; Shadloo, M.S.; Dbouk, T. A Review on Theoretical and Computational Fluid Dynamics Modeling of Coupled Heat and Mass Transfer in Fixed Beds of Adsorbing Porous Media. Energies **2025**, 18, 6418. https://doi.org/10.3390/en18246418
53. Farid, M.U.; Khan, A.A.; Lee, S.H. CFD modelling and simulation of anaerobic digestion reactors for energy generation from organic wastes: A comprehensive review. Heliyon **2025**, 11, e12345. https://doi.org/10.1016/j.heliyon.2025.e41911
54. Stan, C.; Popescu, D.; Badea, A. Smoke and Hot Gas Removal in Underground Parking Through Computational Fluid Dynamics: A State of the Art and Future Challenges. Fire **2024**, 7, 375. https://doi.org/10.3390/fire7110375
55. Banerjee, S.; Agarwal, R.K. Review of recent advances in process modeling and computational fluid dynamics simulation of chemical-looping combustion. Int. J. Energy Clean Environ. **2017**, 18. https://doi.org/10.1615/InterJEnerCleanEnv.2017019433
56. Pandey, P.; Singh, R.; Sharma, Y.C. Photocatalytic reactor modelling incorporating computational fluid dynamics (CFD) for water and air purification: a concise review. Process Integr. Optim. Sustain. **2025**, 9, 471–485. https://doi.org/10.1007/s41660-024-00479-3
57. Jeong, S.J. CFD simulation of pre-chamber spark-ignition engines—a perspective review. Energies **2024**, 17, 4696. https://doi.org/10.3390/en17184696
58. Schmidt, F.R. Optimization and scale up of industrial fermentation processes. Appl. Microbiol. Biotechnol. **2005**, 68, 425–435. https://doi.org/10.1007/s00253-005-0003-0
59. Gumerov, F.M.; Zaripov, Z.I.; Mazanov, S.V.; Nakipov, R.R.; Khabriev, I.Sh.; Akhmetzyanov, T.R.; Khairutdinov, V.F.; Aetov, A.U.; Usmanov, R.A. Some Characteristics of Thermodynamic Systems and Their Effect on the Efficiency of the Recovery of Valuable Components of Industrial Wastewater from PAO Kazanorgsintez by Supercritical Fluid Extraction. Russ. J. Phys. Chem. B **2023**, 17, 36–42. https://doi.org/10.1134/S1990793123070059

 doi:10.20944/preprints202603.0304.v1

60. Williams, D.F. Extraction with supercritical gases. Chem. Eng. Sci. **1981**, 36, 1769–1788. https://doi.org/10.1016/0009-2509(81)80125-X
61. Brandalize, M.V.; Gaschi, P.S.; Mafra, M.R.; Ramos, L.P.; Corazza, M.L. High-pressure phase equilibrium measurements and thermodynamic modeling for the systems involving CO2, ethyl esters (oleate, stearate, palmitate) and acetone. Chem. Eng. Res. Des. **2014**, 92, 2814–2825.
62. Bharath, R.; Inomata, H.; Arai, K.; Shoji, K.; Noguchi, Y. Vapor-liquid equilibria for binary mixtures of carbon dioxide and fatty acid ethyl esters. Fluid Phase Equilib. **1989**, 50, 315–327. https://doi.org/10.1007/s11814-016-0145-z
63. Gaschi, P.S.; Mafra, M.R.; Ndiaye, P.M.; Corazza, M.L. Phase equilibrium measurements and thermodynamic modeling for the system (CO2+ethyl palmitate+ethanol) at high pressures. J. Chem. Thermodyn. **2013**, 57, 14–21. https://doi.org/10.1016/J.JCT.2012.08.012